Silica Reinforcement and Char Reactions in the Apollo Heat Shield

D. E. CAGLIOSTRO,* H. GOLDSTEIN,† AND J. A. PARKER†
NASA Ames Research Center, Moffett Field, Calif.

Reactions of the silica reinforcement fiber and ablation char of the Apollo heat shield have been investigated by laboratory tests in an arc image furnace at temperature levels up to 5000°R, pressures up to 0.7 atm, and heat flux similar to re-entry, 400 Btu/ft² sec, and by an actual re-entry test. Microchemical analyses and x-ray diffraction studies have been made to determine the presence of SiC formation in the char. Experimental data and analytical predictions of thermal and density profiles have been compared for the ablation of virgin heat shield and precharred materials to determine the effects of SiC formation on ablation performance. In all analyses, general agreement was found between chemical composition and the thermal predictions for laboratory tests and re-entry materials. In all ablated materials, SiC was formed in the front surface of the char. The highest SiC content found was 58% by weight and found in a high-pressure environment. The SiC formed was found to act as a heat sink in the ablation process and can lower the front surface temperature by 300°R.

Nomenclature

A = cross-sectional area
C_{ps}, C_{pg} = heat capacity of solid gas
H_g, H_s = enthalpy of the gas, solid
K_s = solid thermal conductivity
M_g = mass flow rates of gas
T = temperature
X = distance from the char surface
θ = time
ρ_s = solid density

Introduction

ABLATORS may contain a source of silica in the form of silicone elastomers or as silica granules or fibers mixed with organic polymer. The silica imparts mechanical strength to the char formed on degradation of the polymer.[1] At elevated temperatures and in anaerobic environments the char carbon and the silica form SiC.[2-7] The formation of SiC is a highly endothermic reaction that can act as a heat sink in the ablation process. Under oxidizing conditions in ablation, both SiC and carbon in the char of the ablator oxidize.[8-10] However, when SiC oxidizes, it reacts to form a surface coat of SiO_2, which protects the underlying carbon or SiC in the char from further oxidation. Carbon alone oxidizes more rapidly than SiC forming the volatile oxides, CO and CO_2, which are lost thereby removing char material. Also, SiC has better mechanical characteristics than carbon[11,12] and can form a tougher char.

Because of the importance of these processes and their potential occurrence at conditions experienced by the Apollo heat shield,[13] the reactions between silica fiber and carbon were investigated. The occurrence of silica-carbon reactions has been investigated primarily in rocket motor linings and phenolic ablators. In the future space shuttle vehicle, SiC coatings have a potential use in protecting carbon nose caps and leading edges.

Received July 22, 1971; revision received December 18, 1971. The authors wish to thank H. Edding for running the x-ray analyses of the Apollo material.

Index categories: Re-Entry Vehicle Testing; Material Ablation; Thermal Modeling and Experimental Thermal Simulation.

* Research Scientist.
† Research Scientist. Member AIAA.

Experimental Procedure

Materials

Material samples were obtained from a re-entered Apollo heat shield and from radiation-only ablation tests conducted in an arc image furnace. Composition and elemental analysis (Table 1) for the virgin material were available from the Manned Spacecraft Center.[14] This elemental analysis is used in all subsequent discussion. Precharred samples tested were obtained by heating the virgin material in 1.0 atm of N_2 at 1930°R (800°C) for 14 hr. The prechars were mounted and run in a similar manner to other samples. A thermogravimetric (T.G.A.) analysis at 3°C/min for virgin heat shield material is shown in Fig. 1.

Arc Image Furnace Runs

Virgin heat shield and precharred material were ablated in helium in an arc image furnace. The samples were 0.5 in. flat-faced cylinders mounted on modified electronic tube sockets (Fig. 2). Heating rates were varied from 200 to 700 Btu/ft²-sec and pressures from 0.001 to 0.7 atm. Detailed descriptions are given in Ref. 15. The test conditions and length of runs are listed in Table 2.

Table 1 Virgin heat shield composition

Virgin polymer Component	Composition Weight fraction
E-glass	0.125
Refrasil	0.125
Phenolic microballoons	0.300
Den-438	0.184
Polysebacic anhydride	0.1962
NMA	0.0346
Vinylcylohexene dioxide	0.0328
DMP-30	0.0023

Virgin polymer Element	Elemental analysis Weight percent
Carbon	50%
Hydrogen	4.5%
Oxygen	16%
Silica	29.5%

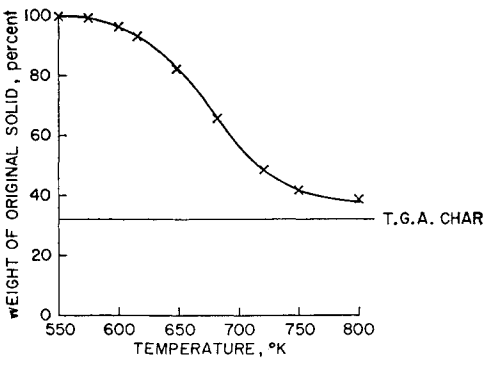

Fig. 1 T.G.A. of Apollo heat shield material.

Fig. 2 Mounted sample.

X-Ray and Chemical Analysis of Materials Tested

Samples of both the Apollo spaceshot materials and the arc image furnace materials were prepared for analysis in similar ways. These samples were designated series 1, 2, and 3. Series 1 and 3 were arc image furnace materials; series 2, Apollo re-entry materials.

For x-ray density gradient measurements, series 1 samples were mounted on a cylindrical tube socket (Fig. 2). A diamond cutoff wheel was used to cut samples $\frac{1}{8}$ in. thick perpendicular to the model. These samples were then placed in a holder for continuous recording of x-ray density gradients.

Series 2 samples were cut from an Apollo space vehicle and soaked in water to remove salts (residuals from sea exposure). They were mounted and cut about $\frac{3}{16}$ in. thick perpendicular to the base with a silicon carbide cutoff wheel. Series 3 samples were prepared in the same way as series 1, except they were $\frac{3}{16}$ in. thick. After the density gradients were recorded, all samples were sectioned to provide powdered material for x-ray diffraction studies to determine the amounts of crystalline materials present. An agate mortar was used to grind these samples to a powder, which was analyzed with a Norelco diffractometer. After the diffraction studies, the powder was submitted for elemental microanalysis. The section locations (Fig. 6) were chosen such that Sec. 1 was the char layer adjacent to the front surface of the char; Sec. 2 was the char layer farther from the front surface; Sec. 3 was the char layer close to the pyrolysis zone; Sec. 4 was the transition zone between char and virgin material; and Sec. 5 was the virgin heat shield material. The experimental density profiles for the ablated materials are calculated from the x-ray absorption profiles. These profiles have been fitted with smooth curves based on a least squares seventh-order polynomial.

Thermal Response Calculations

A modified version of the Aerotherm Corporation's charring material ablator computer program (CMA) has been used to predict and compare thermal performance.[16] The model of an ablating polymer containing silica is composed of three zones; the char, the pyrolysis zone, and the virgin polymer. A schematic for the model is shown in Fig. 3. In the model, heat is transferred or generated by the processes of heat conduction and convection, and by chemical reaction. Mass transfer occurs only by convection and is equivalent to that produced by chemical reaction. Heat flux in the model is applied at the front surface and no recession of this surface occurs. The mass and energy balances are as follows:

Mass Balance

$$\sum_{i=1}^{N} \frac{\partial M_{ig}}{\partial x} = \underbrace{\frac{\partial M_g}{\partial x}}_{\text{change in mass flow}} = \underbrace{\frac{\partial \rho_S}{\partial \theta}}_{\text{mass flow generated by reaction}} \qquad (1)$$

Energy Balance

$$\underbrace{\rho_S C_{ps} \frac{\partial T}{\partial \theta}}_{\text{heat accumulated in solid}} = \underbrace{\frac{1}{A}\frac{\partial}{\partial x}\left(K_S A \frac{\partial T}{\partial x}\right)_\theta}_{\text{heat conducted in solid}} + \underbrace{(H_g - H_S)\frac{\partial \rho_S}{\partial \theta}}_{\text{heat generated by reaction}} + \underbrace{\frac{M_g}{A}\frac{\partial H_g}{\partial x}}_{\text{heat convected by gas}} \qquad (2)$$

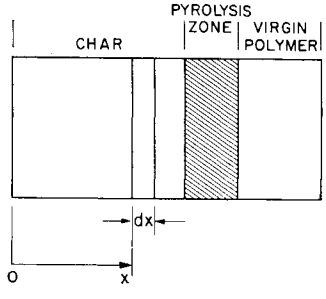

Fig. 3 Ablation model.

Table 2 Sample conditions

Sample	Facility	Average flux Btu/ft²sec	Pressure atm	Atmosphere	Run time sec	Maximum front surface temp °R	Maximum temp 0.1 in. from front surface °R
IA23	Arc image furnace	398	0.00014	He	40	4874°R	2876°R[b]
IA26	Arc image furnace	395	0.0003	He	5	—	—
IA27	Arc image furnace	370	0.0003	He	10	—	—
IA34	1950°R Prechar-arc image furnace	405	0.00017	He	8	4920	2930
IA35	1950°R Prechar-arc image furnace	400	0.00017	He	15	4990	3550
IIA4	MSC	—	—	—	—	—	—
IIA19	Space shot	—	—	—	—	—	—
IIA26	Samples	—	—	—	—	—	—
IIIA21	Arc image	440	0.7	He	40	4610	2650
IIIA49	Arc image	320	0.0002	He	45	3720	3600[a]

[a] Erratic.
[b] Failed at 11 sec.

Table 3 Ablation chemistry-kinetic parameters

Area	Reaction	Kinetic model	Coefficients	ΔH_{RX}, Btu/lb
Pyrolysis zone	Polymer(P) $\longrightarrow$ carbon(C) + pyrolysis gases(PG)	$\frac{dP}{d\theta} = A_1 e^{-E_1/RT(P)}$	$A_1 = 1.75(10^6)$/sec $E_1/R = 2.6(10^4)$	$\Delta H_1 = 500$
Char	Carbon(C) + SiO_2(S) $\longrightarrow$ SiC(SC) + CO)	$\frac{dS}{d\theta} = -A_2 e^{-E_2/RT(S)(C)}$	$A_2 = 2.21(10^3)$ ft^3/lb/sec $E_2/R = 6.25(10^4)$	$\Delta H_3 = 4800$
Char	SiC(SC) $\longrightarrow$ SiC(gaS)	$\frac{d(SC)}{d\theta} = \frac{dS}{d\theta} - A_3 e^{-E3/RT}$	$A_3 =$ ——— $E_3/R =$ ———	$\Delta H_3 = 5950$

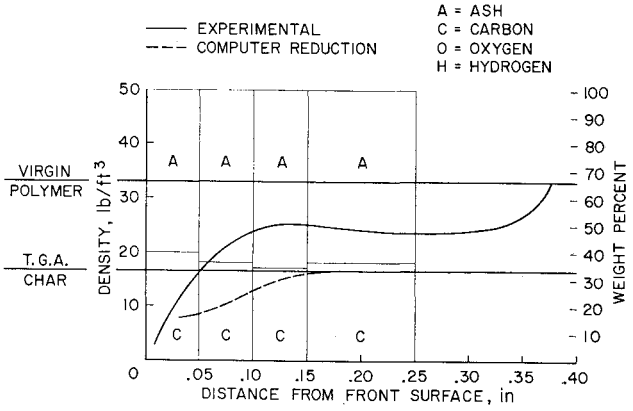

Fig. 4 Sample IA—35 prechar density profile.

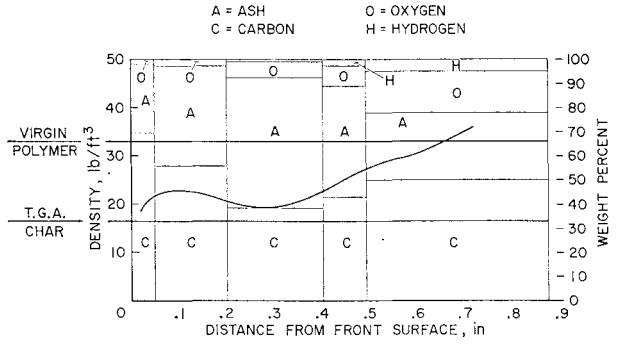

Fig. 5 Sample IIA—19 space shot density profile.

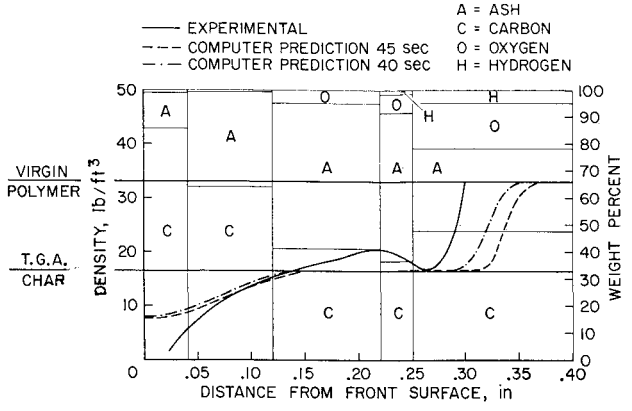

Fig. 6 Sample IIIA—49 virgin polymer density profile.

The assumptions used in this formulation are; 1) gas and solid are in thermal equilibrium, 2) sensible heat can only be accounted for by the solid ($\rho_s C_{ps} \gg p_g C_{pg}$), 3) heat conduction can be accounted for by the solid ($K_s \gg K_g$), and 4) diffusion is slow compared to convection.

These equations are general and can be applied to each of the three zones. It is only necessary to have the proper thermophysical and kinetic data for each zone. In the Apollo material, the important reactions and heats of reaction considered in these zones are shown in Table 3. Little information was available for the sublimation reaction (A_3, E_3/R); therefore, the sublimation option was not exercised. Because there is considerable uncertainty in the kinetic parameters available and used for the SiC reaction (A_2, E_2/R), computer runs were also made with a hundredfold increase in A_2 and a twofold increase in ΔH_2. Computer runs for the polymer pyrolysis and SiC reaction were then compared to runs with just the polymer pyrolysis. Both were then compared to the actual thermal response data obtained from the arc image furnace runs. The differential equations are solved by a finite difference technique. The solution provides gas flow rates and compositions at the char surface, density and temperature profiles within the solid, and the location of the pyrolysis zone.

Results and Discussion

A typical experimental density profile for each of the different ablated materials is shown in Figs. 4–6. The limiting values shown are for the density of virgin heat shield material and the char density obtained from thermogravimetric analysis experiments up to 800°C. While the virgin material was sometimes more dense than manufacturer's data would suggest, the char density after ablation was less than expected for a loss of material due to pyrolysis and SiC formation. Visual examination and x-ray diffraction data show evidence of voids and shrinkage and point to a physically inhomogeneous char and pyrolysis zone (see Fig. 7). It may be

Fig. 7 Cross section of a spaceshot char.

concluded that the inhomogeneities result from the ablation process itself which sets up thermal and mechanical strains that deform the material. In one spaceshot sample, further evidence was apparent in the formation of long fissures spanning the entire length of the original sample (Fig. 7).

The elemental composition of the char and virgin heat shield material are shown in Figs. 4 and 6, respectively. These values are within the ranges expected from the manufacturer's specifications. In all cases the ablated materials contained SiC in the areas close to the front surface of the char. In arc image furnace runs, the surface temperatures of the chars were in the range where SiC formation should occur. In Fig. 8, typical results of the SiC analysis and temperature histories available are shown along with the temperatures for SiC formation and sublimation and melting point of SiO_2. The remaining data on SiC content are shown in Table 4. In one sample from the arc image furnace runs (A21 series 3), the section close to the front surface of the char contained 50% SiC. This run differed from the remaining runs because it was made at a relatively high pressure 0.7 atm and had a front surface temperature of 4610°R. The high SiC content may result from the suppression of SiC sublimation at the higher pressures. All results are for the crystalline form of SiC and therefore represent a lower limit on the total concentration of SiC present because noncrystalline SiC may also be present. The error in the weight percent reported for the crystalline material is ±10%. When prechars fired at 800°C were ablated in the arc image furnace, SiC was also formed in the section close to the front surface. In these samples, little change was observed in the total weight percent of carbon. If silica and carbon react to form SiC, there is only a small change in the total carbon content of the sample (i.e., for the reaction).

$$SiO_2 + 3C \longrightarrow SiC + 2CO$$

At 100% conversion of the limiting reactant SiO_2, the carbon content in the solid would decrease from 39.4 to 34.6% by weight (including the carbon present in the SiC formed). There is a large difference between the carbon compositions of the front layer of char from the ablation materials derived from virgin heat shield ablation and from prechar ablation. After ablation, the carbon content in prechars does not exceed 40% by weight (Fig. 4), but in the virgin heat shield materials, the carbon content close to the front surface is greater than 40% (Fig. 6). This implies that SiO_2 is being removed by other processes as well as by reaction with the carbon in the char to form SiC; alternatively, there may be secondary deposition of carbon from the polymer pyrolysis gases in the char. For example, if SiO_2 vaporizes to gaseous SiO and this gaseous SiO is a precursor in the reaction to produce SiC, SiC formation could be limited by the physical removal of SiO gas by entrainment in the transpiring gases

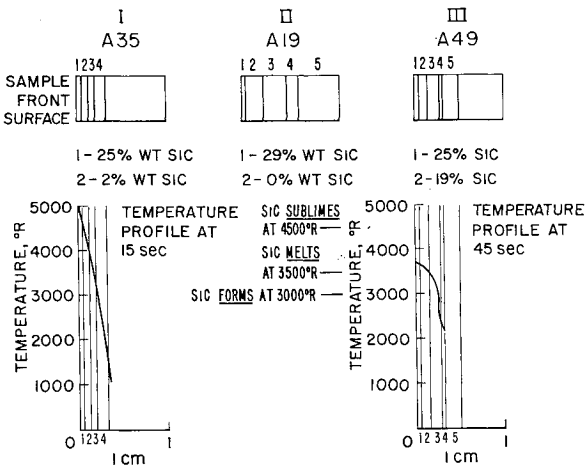

Fig. 8 Thermal history of samples.

Table 4 SiC content of char

Run	Maximum % by weight crystalline SiC[a] wt. % SiC
I A26	9%
I A27	21%
I A34	24%
I A35	25%
II A19	29%
II A26	9%
II A4	2%
III A21	58%
III A49	25%

[a] In all samples maximum SiC was found to occur in area adjacent to front surface of char.

from the pyrolyzing polymer. These transpiring gases might also blow the molten silica away from the char, or actually react with the SiO gas, thus reacting in the gas phase and inhibiting the reaction of SiO with the solid carbon in the char. In the case of secondary carbon deposition, the density near the front surface may decrease by sublimation, reaction, or physical loss, while pyrolysis gases are cracked depositing carbon. The density would thus decrease as shown in the sections close to the front surface, yet the carbon content would increase.

Thermal Response

The temperature response for the runs in the arc image furnace are reported for representative samples in Figs. 9–12. These profiles show the thermal response at various depths and at the front surface of the char. The two prechar samples were run at similar conditions of heat flux and pressure to check the reproducibility of the arc image furnace experiments. The measured temperature profiles compared in Fig. 9 agree within ±50°C. The virgin polymer heat shield material provides more thermal protection than the char alone, as would be expected. A thermal response curve for the virgin polymer heat shield is compared to the response of the prechar in Fig. 10. Computer predicted thermal response curves derived from the analytical model have also been plotted in Figs. 11 and 12. While these profiles are predicted in depth, the predictions are usually high for both the virgin heat shield aterial and the prechars. Possible reasons for this are that the chars formed are inhomogeneous and therefore the thermophysical data are not adequate, or that not all the chemical and physical phenomena are included in the model. The model does give a conservative prediction and can therefore be used in designing adequate heat shield thicknesses. In addition to the computer prediction, which includes only the virgin polymer pyrolysis kinetics, plots have been made that also include the SiC kinetics. Figures 11 and 12 show that including the SiC endothermic reaction can decrease the

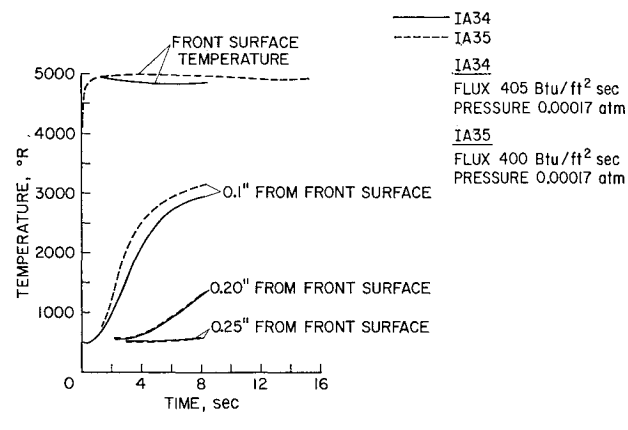

Fig. 9 Samples IA34 and IA35 prechars.

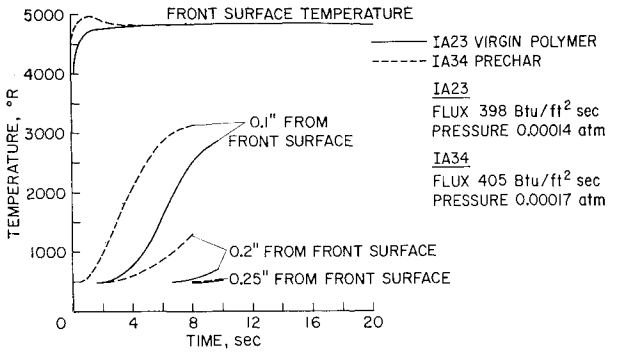

Fig. 10 Samples IA23 and IA34.

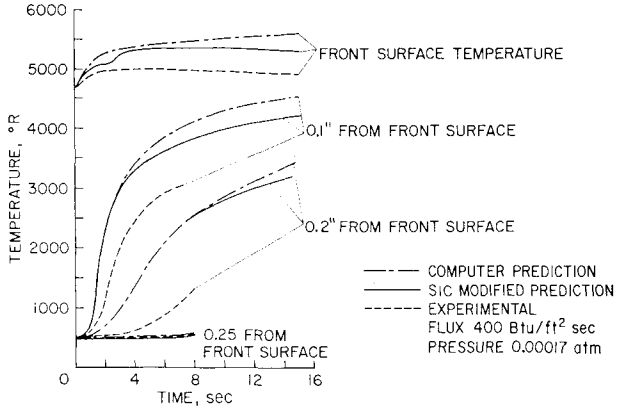

Fig. 11 Sample IA35 prechar.

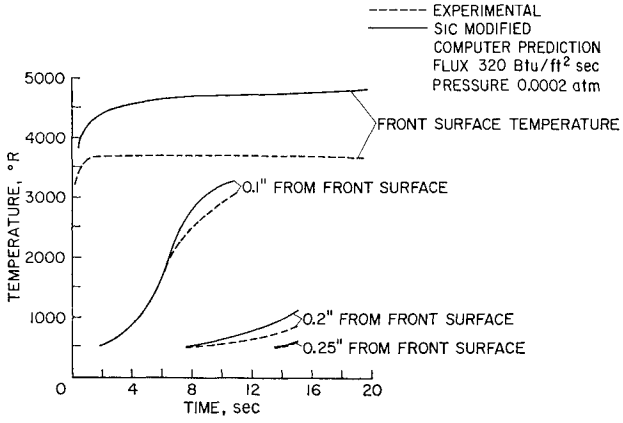

Fig. 12 Sample IIIA49 virgin polymer.

temperature response predicted for the materials and that the reaction can decrease the front surface temperature of the char by about 300°R (Fig. 11).

A fact to note from the computer predictions is that they all predict temperatures at the front surface that are too high compared to experiment. At these elevated temperatures, additional phenomena occur and should be taken into account in the analytical model. For example, although the model predicts a temperature of 2897°C (5200°R) (Fig. 11), the model does not include the reactions of SiC sublimation and dissociation and SiO_2 dissociation and vaporization. All these processes can also occur at these temperatures. Unfortunately, they occur at very high temperatures, and accurate chemical parameters describing them are difficult to obtain with direct experiment. Further experimental information will be required to include these phenomena. The analytical model is flexible enough so this experimentation can be included easily once the problem of obtaining high-temperature rate data is solved.

Summary

Silica reactions with carbon in the Apollo heat shield have been investigated in an actual re-entered heat shield and in samples produced with an arc image furnace. In all cases, x-ray diffraction studies show that SiC is formed in the front surface of the char. Chemical analyses of virgin polymer ablation samples show that the amount of total residual carbon in the chars differs from that in prechar ablation samples. This difference was attributed to chemical reaction or physical removal of SiO_2 from the char or to secondary deposition of carbon from the pyrolysis gases.

A computer model of the ablation process shows that incorporation of the SiC reaction sequence acts as a heat sink and decreases front surface temperatures and in-depth temperatures. The computer predictions also indicate that the temperatures attained near the front surface may be sufficiently high for other processes to occur at the high temperatures of the char. Therefore, modifications of the model should be made to test the effects of reactions such as SiC dissociation and sublimation, and SiO_2 vaporization.

References

[1] Pope, R. B., Riccitiello, S. R., and Parker, J. A., "Experimental Evaluation of Polyurethane Foam Composites for Low Heating-Rate Thermal Protection," *Journal of Spacecraft and Rockets*, Vol. 6, No. 4, April 1969, pp. 506–508.

[2] Klinger, N., Strauss, E. L., and Komarek, K. L., "Reactions Between Silica and Graphite," *Journal of the American Chemical Society*, Vol. 49, No. 7, July 1966, pp. 369–375.

[3] Romie, F. E., "Carbon-Silica Reaction in Silica-Phenolic Composites," *AIAA Journal*, Vol. 5, No. 8, Aug. 1967, pp. 1511–1513.

[4] Rindal, R. A. and Moyer, C. B., "Comment on Carbon-Silica Reaction in Silica-Phenolic Composites" *AIAA Journal*, Vol. 6, No. 5, May 1968, pp. 991–992.

[5] Beecher, N. and Rosensweig, R. E., "Ablation Mechanisms in Plastics With Inorganic Reinforcement," *ARS Journal*, April 1961, pp. 532–539.

[6] Blumenthal, J. L., Santy, M. J., and Burns, E. A., "Kinetic Studies of High-Temperature Carbon-Silica Reactions in Charred Silica-Reinforced Phenolic Resins," *AIAA Journal*, Vol. 4, No. 6, June 1966, pp. 1053–1057.

[7] Rosensweig, R. E., "Theory for the Ablation of Fiberglass-Reinforced Phenolic Resin," *AIAA Journal*, Vol. 1, No. 8, Aug. 1963, pp. 1802–1809.

[8] Gaydon, A. G. and Wolfhard, H. G., *Flames — Their Structure, Radiation, and Temperature*, Chapman & Hall Ltd., London, England, 1960, pp. 175–209.

[9] Mantell, C. L., *Carbon and Graphite Handbook*, Interscience, New York, 1968, p. 167.

[10] O'Connor, J. R. and Smildens, J., *Silicon Carbide — A High Temperature Semiconductor*, Pergamon Press, New York, 1960, pp. 235–250.

[11] Materne, H. P. and Kuhbander, R. J., "Silicon Carbide Filament Reinforced Epoxy Resin Composites," *Proceedings of the 10th National Symposium and Exhibit*, San Diego, Calif., *SAMPE*, Vol. 10, Nov. 10–11, 1966, p. A–32.

[12] Hawkins, H. T. and Schmidt, D. L., "Bicompositional Carbon-Silica Fibers," *Proceedings of the 10th National Symposium and Exhibit*, San Diego, Calif., *SAMPE*, Vol. 10, Nov. 10–11, 1966, p. D–66.

[13] Curry, D. M. and Stephens, E. W., "Apollo Ablator Thermal Performance at Superorbital Entry Velocities," TN D–5969, 1970, NASA.

[14] "Evaluation of the Thermophysical Properties of the Apollo Heat Shield," AVCO Rept. AVSSD–0375–67–RR, NAS 9–6940, Aug. 8, 1967, AVCO Missiles Space & Electronics Group, Lowell Industrial Park, Lowell, Mass.

[15] D'Alelio, G. F. and Parker, J. A., *Ablative Plastics*, Marcel Dekker Inc., New York, 1971, pp. 380–385.

[16] Moyer, K. B., et al., "Description of Relevant Aerotherm Programs," Corp. Rept., July 1970, Aerotherm Corp., Mountain View, Calif., pp. 5–11.